Contribution of nanointerfaces to colossal permittivity of doped $Ba(Ti,Sn)O_3$ ceramics

Oleg V'yunov, Borys Reshytko, Anatolii Belous & Leonid Kovalenko

Applied Nanoscience

ISSN 2190-5509

Appl Nanosci
DOI 10.1007/s13204-018-0743-7

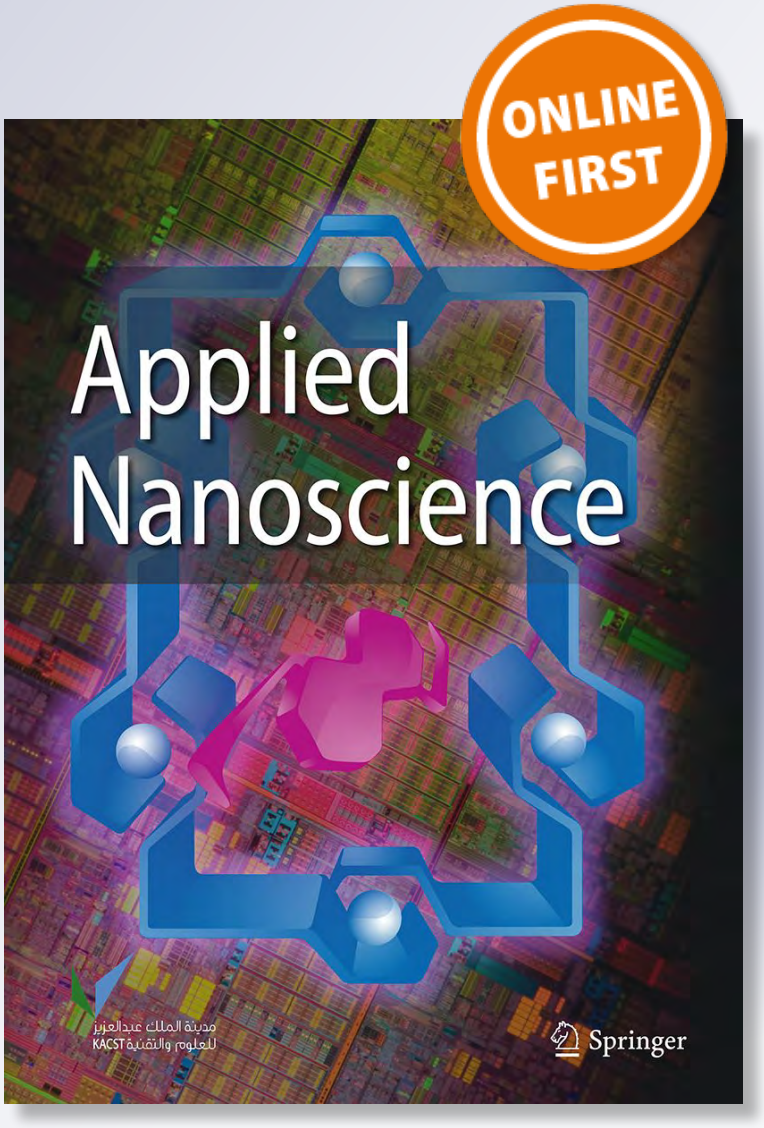

Springer

Applied Nanoscience
https://doi.org/10.1007/s13204-018-0743-7

ORIGINAL ARTICLE

Contribution of nanointerfaces to colossal permittivity of doped $Ba(Ti,Sn)O_3$ ceramics

Oleg V'yunov[1] · Borys Reshytko[1] · Anatolii Belous[1] · Leonid Kovalenko[1]

Received: 28 December 2017 / Accepted: 21 March 2018

Abstract
The microstructure, crystal chemical parameters and electrical–physical properties of samples of barium titanate-based dielectric and semiconductor ceramics were investigated in a wide frequency range. The contributions of different nanointerfaces to the permittivity of samples under investigation have been determined.

Keywords Semiconductor barium titanate · Colossal permittivity · Microstructure · Nanointerface at grain boundaries · Metal–dielectric nanointerface

Background

In recent years, the materials having colossal permittivity ($\varepsilon > 1000$) have been of particular scientific and practical interest (Krohns et al. 2009). The use of such materials makes it possible to solve the problems of microminiaturization of electronic circuits and to develop on their basis energy-storage devices. The materials with high permittivity are generally developed on the basis of ferroelectric materials. The high permittivity in ferroelectrics is due to spontaneous polarization, a domain structure and mobile domain walls. Besides the ferroelectric polarization mechanism, there are other polarization mechanisms, which can lead to an increase in ε, for example: charge density wave formation (Dumas et al. 1983; Littlewood 1987), hopping conduction mechanism (Zheng et al. 2013), occurrence of the metal–dielectric transition (Hess et al. 1982), as well as various mechanisms, which can occur only on oxide system containing transition metals (Lunkenheimer et al. 2002; Lunkenheimer et al. 2009).

A considerable member of the above polarization mechanisms (e.g., ferroelectric polarization, hopping conduction mechanism, occurrence of the metal–dielectric transition, as well as internal interface at the grain boundaries) can manifest themselves in ferroelectric semiconductors based on barium titanate ($BaTiO_3$), which crystallizes into a perovskite structure (Guillemet-Fritsch et al. 2008; Wu et al. 2015). Dielectric barium titanate, in which titanium is only in the oxidation state 4+: $Ba^{2+}Ti^{4+}O_3$, acquires semiconductor properties on the addition of donor impurities, which results in the partial reduction of titanium ($Ti^{4+} \rightarrow Ti^{3+}$) (Belous et al. 1997; V'yunov et al. 2006). When the material is synthesized in an air atmosphere, it becomes homogenous in electrical and physical properties; the grain interior acquires semiconductor properties, and the grain boundaries exhibit dielectric properties because of oxygen diffusion along the grain boundaries, which is accompanied by the reduction of Ti^{3+} to Ti^{4+} (Belous 2008). Using *n*-type dopants with high solubility in $BaTiO_3$, for example, rare earth elements with mean ionic radius: Y, Dy, Ho (Xue et al. 1988), one can obtain materials with reproducible properties, e.g., $(Ba^{2+}_{1-x}Y^{3+}_{x})(Ti^{3+}_{1-x}Ti^{4+}_{x}Sn^{4+}_{x})O_3$. For example, in the case of yttrium, semiconductor properties appear in a wide concentration range with the minimum at an impurity content of 0.4 mol% (Belous et al. 2003). Inhomogeneity of semiconducting barium titanate in electrical and physical properties can be increased using acceptor impurities (e.g., Mn, Fe, Cr, Cu), which are not part of the perovskite

✉ Oleg V'yunov
vyunov@ionc.kiev.ua

Borys Reshytko
reshytko@ionc.kiev.ua

Anatolii Belous
belous@ionc.kiev.ua

Leonid Kovalenko
leo_kov@ukr.net

[1] V. I. Vernadskii Institute of General and Inorganic Chemistry of the NAS of Ukraine, 32/34 Palladina Ave., Kiev 03142, Ukraine

Published online: 29 March 2018

structure, but create acceptor levels at the grain boundaries, increasing the electrical resistance of the grain boundaries and forming potential barriers (V'yunov et al. 2003), that is, the nanosize interfaces, whose size is about 16 nm, are formed at grain boundaries (Wang 1994). Besides, increasing the acceptor's concentration at the boundary increases the height of the grain potential barriers (nanointerfaces with a width of 5 nm) at the boundary between the material and electrode. Therefore, it is important to determine the contribution of nanosize interfaces to the value of permittivity and dielectric loss. V'yunov et al. (2017) shows the contribution of mechanisms in the ferroelectric temperature range, but in this range the contribution of ferroelectric mechanisms is small. The largest contribution can be observed in the region of the ferroelectric–paraelectric phase transition. The point of the phase transition can be shifted towards room temperature by the particle substitution of Ba^{2+} ions by Sr^{2+}, or of the Ti^{4+} ion by the Sn^{4+} and Zr^{4+} ions (Hou et al. 2016). In case of Zr, the maximum value decreased to 8×10^3 relative to pure barium titanate [10^4 (Yang et al. 2016)]; in case of Sr it increases to 10×10^4 and in case of Sn to 14×10^4 (Fricbergs 1971; Von Hippel et al. 1946). Thus, maximum permittivity value can be obtained from Sn; therefore, Sn was chosen as a dopant for the research. At room temperature, $Ba(Ti_{1-x}Sn_x)O_3$ solid solution has cubic crystal symmetry at $x=0.15$ (Xiaoyong et al. 2003; Yasuda et al. 1996).

The aim of this study was to synthesize dielectric $Ba(Ti_{0.85}Sn_{0.15})O_3$ and semiconducting $(Ba_{0.996}Y_{0.004})(Ti_{0.85}Sn_{0.15})O_3$ barium titanates to investigate their electrical and physical properties in a wide frequency range and to determine the contributions of nanosize interfaces (at the grain boundaries and at the metal–dielectric boundary) to permittivity.

Methods

Methods of synthesis

Ultrapure $BaCO_3$, $SnCO_3$, TiO_2, Y_2O_3 and SiO_2 were used as starting reagents for the synthesis. To effect sintering with the participation of a liquid phase, TiO_2 was added (2 at.% excess over the stoichiometric amount) (Drofenik 1993). A small amount of SiO_2 was added as an impurity to reduce the sintering temperature (Glinchuk et al. 2000). The starting reagents were dried to remove moisture. The grinding was carried out on a GKML-16 vibrating mill (Hungary) in agate drums using chalcedony balls. After that, the mixture was dried in a drying cabinet. The synthesis temperature was determined by the amount of the free barium oxide in the resulting mixture; after heat treatment, its concentration was less than 1%. For the uniform distribution of manganese, which acts as an acceptor of impurity in semiconducting $(Ba_{0.996}Y_{0.004})(Ti_{0.85}Sn_{0.15})O_3$ barium titanate, manganese was added by precipitation from solutions using $MnSO_4$ and an aqueous solution of ultrapure ammonia. After synthesis and subsequent grinding, perovskite was mixed with an organic binder (10% polyvinyl alcohol), pressed by uniaxial pressing at 150 MPa into disks 10 mm in diameter and 3 mm in thickness and sintered at ~ 1350 °C. The active reduction of titanium and high density of samples served as a criterion for the choice of sintering temperature, and the cooling rate used provided oxidation only of the grain boundaries.

Characterization

The X-ray phase analysis was performed on DRON-4-07 diffractometer (Co *K*α radiation). The structural parameters of polycrystalline samples were determined by the Rietveld analysis. The X-ray data were recorded in the scan range $2\Theta=10°–150°$ with the step $\Delta2\Theta=0.04°$ and an exposure time 6 s. SiO_2 (2Θ standard) and Al_2O_3 (intensity standard) were used asexternal standards.

The size of crystallites was studied by means of laboratory equipment based on an SEC mini-SEM SNE-4500 MB, desktop scanning electron microscope equipped with EDS spectrometer EDAX Element PV6500/00 F and SC7620 'Mini' Sputter Coater.

The ohmic and blocking contacts were obtained by firing an aluminum paste and a silver paste, respectively. The measurements of the electrical properties were made at direct and alternating current at the room temperature and at an electric field strength of 50 mV/mm. The complex impedance relations $Z=Z'+iZ''$ (where Z' and Z'' are real and imaginary parts of complex impedance) in a wide frequency range (1 Hz–1 MHz) were obtained using a 1260A Impedance/Gain-Phase Analyzer (Solartron Analytical). The equivalent circuit and the value of its components were determined using ZView® for Windows (Scribner Associates Inc., USA).

Results and discussion

To determine the intermediate phases that are formed during the synthesis of the dielectric $Ba(Ti_{0.85}Sn_{0.15})O_3$ and semiconducting $(Ba_{0.996}Y_{0.004})(Ti_{0.85}Sn_{0.15})O_3$ barium titanate by the solid-state method, an isothermal heat treatment of powders in a temperature range of 600–1100 °C was carried out. The X-ray diffraction patterns of a mixture of powders of dielectric and semiconducting barium titanate exhibit reflections of several phases after heat treatment at temperatures below the synthesis temperature (1100 °C). The perovskite phase predominates over the entire temperature range. The

Table 1 Structural parameters of ceramic samples

	$Ba(Ti_{0.85}Sn_{0.15})O_3$	$(Ba_{0.996}Y_{0.004})(Ti_{0.85}Sn_{0.15})O_3 + 0.004$ mol% Mn
Unit cell parameters		
a (Å)	4.02251(4)	4.02254(4)
V (Å^3)	65.086(1)	65.088(1)
Agreement factors		
R_b (%)	3.85	4.01
R_f (%)	2.12	2.87

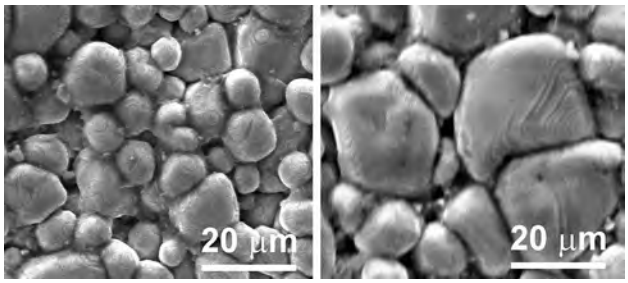

Fig. 2 Microstructure of the $(Ba_{0.996}Y_{0.004})(Ti_{0.85}Sn_{0.15})O_3$ (**a**) and $Ba(Ti_{0.85}Sn_{0.15})O_3$ (**b**) ceramics, ×1000 magnification

intermediate phases in the synthesis were barium orthotitanate (Ba_2TiO_4) and barium tetratitanate ($BaTi_4O_9$). After heat treatment at 1100 °C both samples consisted of single phase within the accuracy of the X-ray method (1 wt%). The crystal structure parameters of the samples (Table 1) were determined by the Rietveld structural analysis (Fig. 1). After sintering at 1360 °C in air atmosphere, they crystallize into a perovskite structure with a space group Pm-3m (№ 221) and ion positions [Ba(Y) 1b (½ ½ ½), Ti(Sn) 1a (0 0 0); O 3d (½ 0 0) (Tilley 2006)].

The ceramic samples of dielectric barium titanate have grain sizes of ~ 10 μm (Fig. 2a). At the same time, in semiconducting barium titanate, the grain size is much larger (~ 35 μm), which is attributed to an abnormal grain growth in the presence of a liquid phase (Drofenik et al. 2002), which is formed due to a eutectic in the 49.5 mol% BaO–50.5 mol% TiO_2 system with the melting point of 1322 °C (Toropov 1969). When manganese is added to semiconducting barium titanate, the mean grain size of the ceramics does not practically change.

The band diagram of the metal–semiconductor contact, which is formed by applying different electrodes (Al, Ag) to a $(Ba_{0.996}Y_{0.004})(Ti_{0.85}Sn_{0.15})O_3$ sample, was constructed (Fig. 3) using the following values: band gap in barium titanate $E_g = 3$ eV (Vul et al. 1973), in barium stannate $E_g = 3.4$ eV (Wu et al. 2017), doping with *n*-type dopants shifts the Fermi level by 0.1 eV in the direction of the conduction band (Dawber et al. 2001), the electron work function of a semiconducting barium titanate $A_{sc} = 4.4$ eV and the band gap $E_g = 3.1$ eV (Marikutsa et al. 2015), and the electron work function of aluminum and silver $A_{Al} = 4.2$ and $A_{Ag} = 4.7$ eV (Nikolsky 1982).

In the case of an aluminum electrode, the electron work function of the metal is smaller than that of the semiconductor, $A_{Sc} > A_M$ (Fig. 3a). In the contact region, electrons will pass from the metal to the semiconductor, and the electron concentration in the contacting semiconductor layers will increase (enriched layer). On the metal–semiconductor interface, an ohmic contact is formed.

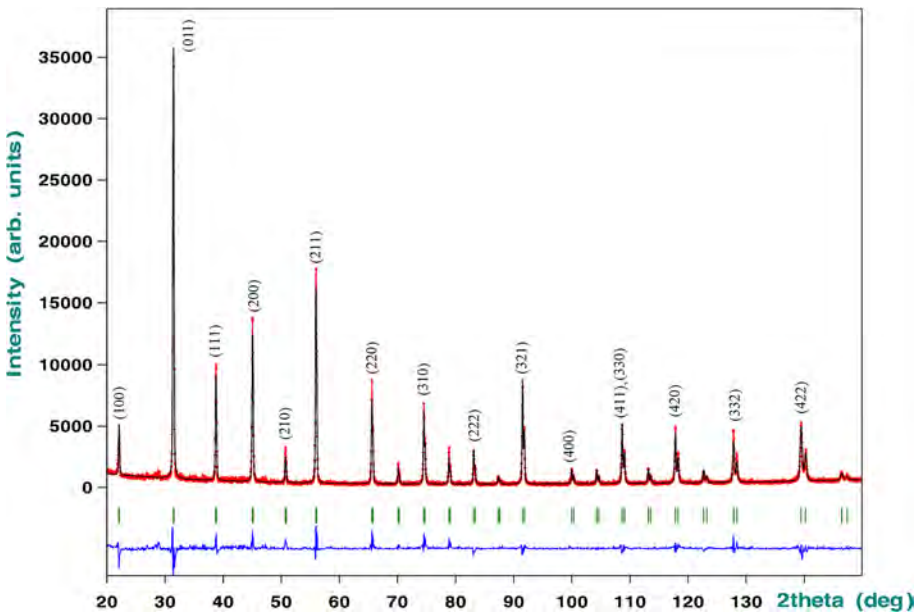

Fig. 1 Experimental (points) and calculated (lines) X-ray powder diffraction patterns of the $(Ba_{0.996}Y_{0.004})(Ti_{0.85}Sn_{0.15})O_3$ ceramics. Vertical bands indicate the positions of the peaks; the Miller indices are in parentheses. The difference curve is shown below

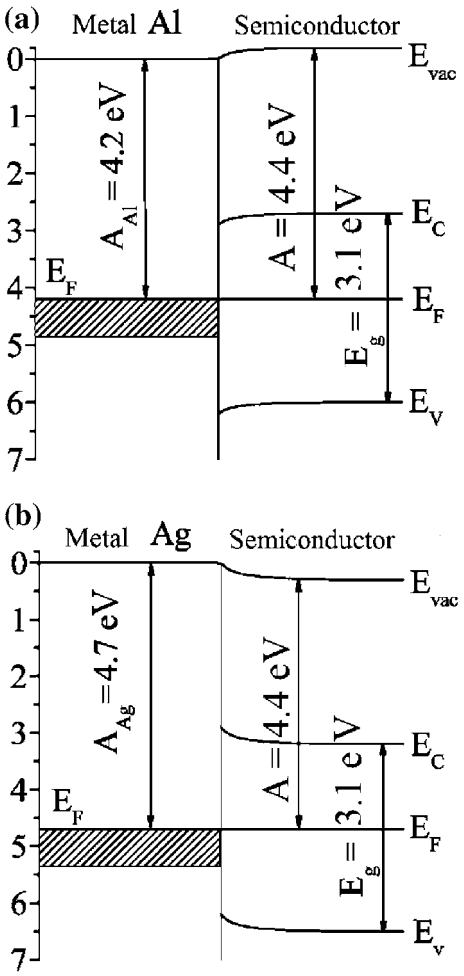

Fig. 3 Band diagram of the metal–semiconductor contact, which is formed on applying different electrodes: Al (**a**), Ag (**b**) to a $(Ba_{0.996}Y_{0.004})(Ti_{0.85}Sn_{0.15})O_3$ sample

In the case of using electrodes based on silver, the electron work function of the metal is larger than that of the semiconductor $A_{Sc} > A_M$ (Fig. 3b). In the contact region, electrons will pass from semiconductor to the metal; in the contacting semiconductor layer, the electron concentration will decrease (depleted layer). The so-called Schottky barrier is formed at the interface (a blocking contact).

The use of ohmic or blocking electrodes (Ag) affects the impedance diagram. In the case of an ohmic contact (Al), a semicircle is observed (Fig. 4, curve 1), and in the case of blocking (Fig. 4, curve 2), an additional element, a vertical or an inclined straight line relating to processes at the metal–semiconductor boundary appears (Fig. 4). In the case of an ohmic contact (Al), the real part of impedance (Z') at $f = 0$ Hz (Fig. 4) corresponds to the DC resistance of the sample. The conductivity of semiconducting barium titanate decreases with increasing manganese concentration, which is associated with an increase in potential barriers at the

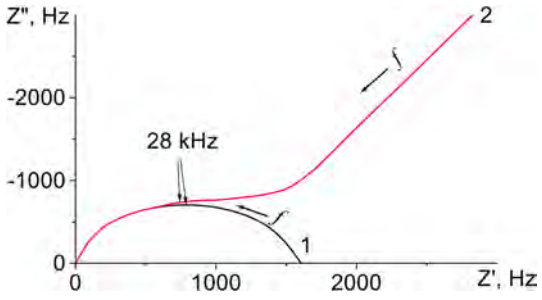

Fig. 4 Complex impedance of a $(Ba_{0.996}Y_{0.004})(Ti_{0.85}Sn_{0.15})O_3$ sample with ohmic Al (1) and blocking Ag (2) electrodes

grain boundaries. It is known that the conductivity of semiconductors varies exponentially as a function of potential barrier height, which is proportional to the ratio of electrons in the grain interior and at the boundaries (V'yunov et al. 2003). Figure 5 shows equivalent circuits and a schematic representation of the microstructure barium titanate-based dielectric $Ba(Ti_{0.85}Sn_{0.15})O_3$ and semiconductor $(Ba_{0.996}Y_{0.004})(Ti_{0.85}Sn_{0.15})O_3$ ceramics. In the case of dielectric barium titanate, the grain boundary and interior have dielectric properties. Dielectric characteristics of ceramics with nanosized grains can change several times compared to single crystal (Hirose and West 1996; Buscaglia et al. 2006). When the grain sizes are 10 μm or more, the influence of grain boundaries on the permittivity is not significant (Arlt et al. 1985). In this case, the equivalent circuit is represented by one RC element (Okadzaki 1976). The microstructure of semiconducting barium titanate is complex; the grain interior is of semiconducting nature, and the grain boundaries are of dielectric nature, which results in the formation of capacitor at each dielectric boundary (Fig. 5b). The use of the constant phase element (CPE) is caused by the necessity of taking into account the distribution of the values of the resistance of grain boundaries and their capacities (Sluyters-Rehbach 1994).

Besides, in the case of blocking electrode, an additional capacity is formed at the electrode–semiconductor boundary.

The obtained frequency dependencies ($Z'' = f(Z')$) for the tin-doped $(Ba_{0.996}Y_{0.004})(Ti_{0.85}Sn_{0.15})O_3$ ceramic can be analyzed in the form of four types of frequency dependencies: complex impedance (Z^*), complex admittance (Y^*), complex dielectric constant (ε^*) and complex electrical modulus (M^*). The complex quantities are connected by the relation $M^* = 1/\varepsilon^* = j\omega C_0 Z^* = j\omega C_0 / Y^*$, where $j = \sqrt{-1}$. To calculate the permittivity and dielectric losses, the following relations were used: tg $\delta = Z'/Z''$, $Y'' = Z''/(Z'^2 + Z''^2)$, $\varepsilon' = Y''/2\pi f \varepsilon_0$, where $\omega = 2\pi f$ (where f is frequency, Hz) and ε_0 is a dielectric constant (8.854×10^{-14} F/cm).

Figure 6 shows the calculated values of the effective permittivity and dielectric loss (ε', tg δ) of dielectric $Ba(Ti_{0.85}Sn_{0.15})O_3$ and semiconducting $(Ba_{0.996}Y_{0.004})(Ti_{0.85}Sn_{0.15})O_3$ barium

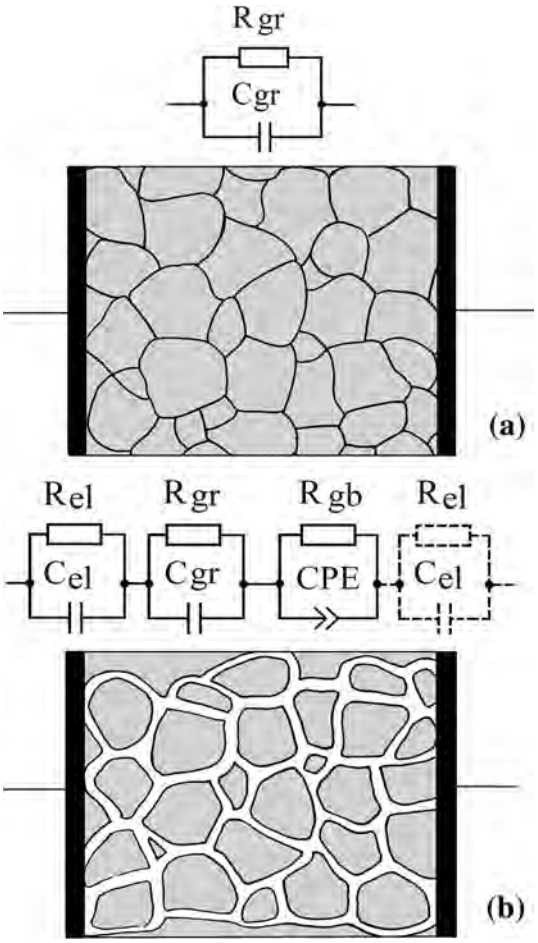

Fig. 5 Equivalent circuits and schematic representation of the microstructure of dielectric $Ba(Ti_{0.85}Sn_{0.15})O_3$ (**a**) and semiconductor $(Ba_{0.996}Y_{0.004})(Ti_{0.85}Sn_{0.15})O_3$ (**b**) ceramics. C_{el}, R_{el}, R_{gr}, C_{gr}, R_{gb} and CPE are the resistance and the capacity of the electrodes, the volume and grain boundaries, respectively. Elements of the circuit that simulate the wires are not shown for simplicity

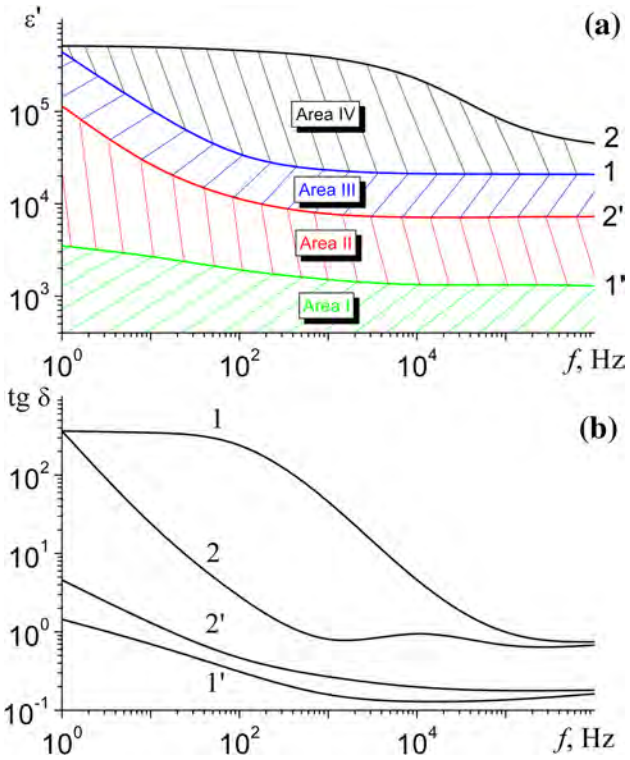

Fig. 6 Dielectric permittivity (ε') and dielectric losses (tg δ) of semiconductor $(Ba_{0.996}Y_{0.004})(Ti_{0.85}Sn_{0.15})O_3 + 0.004$ mol%. Mn (1), $(Ba_{0.996}Y_{0.004})(Ti_{0.85}Sn_{0.15})O_3$ (2,2′), and dielectric $Ba(Ti_{0.85}Sn_{0.15})O_3$ (1′) samples with aluminum (ohmic) (1) and silver (blocking) (1′, 2, 2′) electrodes

titanate samples with silver (blocking) and aluminum (ohmic) electrodes. In the case of a dielectric barium titanate with different electrodes, the permittivity and dielectric loss do not vary with frequency and are much lower than in semiconducting barium titanate, which is attributed to the absence of capacitors that are formed at the grain boundary and to a relatively small contribution of nanointerface at the metal–dielectric boundary, and are practically independent of the type of the electrodes (curves 1′, 2′). As it is seen from Fig. 6, for dielectric barium titanate, ferroelectric polarization gives the main contribution to the permittivity value (area I). The electrodes practically do not affect either the permittivity or the dielectric loss; the curves 1′ and 2′ almost coincide (Fig. 6a, b, respectively).

The permittivity of semiconducting $(Ba_{0.996}Y_{0.004})(Ti_{0.85}Sn_{0.15})O_3$ barium titanate with silver electrodes (curve 2) does not practically change over a wide frequency range (up to 10^4 Hz). At the same time, as in the case of using ohmic contacts, the effective permittivity of semiconducting barium titanate changes sharply (curve 1). This difference in the frequency dependence of permittivity may be attributed to an additional capacity, which appears at the metal–semiconductor nanointerface when silver is used as the electrode (blocking electrode). For practical applications, the absence of permittivity changes in a wide frequency range is important. It should be noted that when using blocking (silver) contacts, the permittivity changes only slightly, and a low dielectric loss as compared with the use of ohmic contacts is observed, which is also important for practice.

In the case of semiconducting barium titanate with aluminum electrodes, the contribution of ferroelectric polarization is close in the order of magnitude to that in dielectric material (Fig. 6a, area I). Hopping conduction and nanointerfaces at the grain boundaries give a considerable contribution to permittivity (area II, III). Their contributions were distinguished using the calculated values for sample $(Ba_{0.996}Y_{0.004})(Ti_{0.85}Sn_{0.15})O_3$ and for the sample of the same composition, but with additional Mn dopant (Fig. 6b). Figure 6b shows that the contribution of the hopping conductivity is much larger than the contribution of nanointerfaces

at grain boundaries. The contribution of nanointerfaces at metal–semiconductor boundaries for semiconducting barium titanate with silver electrodes (area IV) ensures a constant ε value in a wide frequency range (curve 2). From Fig. 6 and calculations using equivalent circuits it is evident that the mechanisms change in decreasing order of contribution to the permittivity as follows: nanointerface at grain boundaries, hopping conduction, electrode nanointerface (in the case of a blocking (Ag) electrode), and ferroelectric polarization. A permittivity dispersion is also observed independent of electrode.

Conclusions

Samples of dielectric and semiconducting barium titanate have been synthesized; investigations of their electrical and physical properties have been carried out. It has been shown that in semiconducting barium titanate, effective permittivity greatly increases compared with dielectric barium titanate because of the formation of nanointerfaces at the grain boundaries and electrode–semiconductor nanointerface if blocking electrodes (Ag) are used.

Acknowledgements The work was carried out with the financial support from the research program of the Ukrainian National Academy of Sciences "New functional substances and materials for chemical production" (Fine Chemicals).

Author contributions OV performed X-ray powder diffraction and SEM investigations and took part in analyzing the obtained results, BR carried out calculation of zone diagrams and fitted impedance data using equivalent circuits, KL synthesized ceramic samples, performed mechanical treatment of the samples, and collected data of complex impedance. OV, BR and KL contributed in the drafting and revision of the manuscript. AG supervised the work and finalized the manuscript. All authors read and approved the final manuscript.

Compliance with ethical standards

Conflict of interest The authors declare that they have no competing interests.

References

Arlt G, Hennings D, De With G (1985) Dielectric properties of fine-grained barium titanate ceramics. J Appl Phys 58(4):1619–1625

Belous AG, Vyunov OI, Yanchevski OZ, Kovalenko LL (1997) Thermodynamic and experimental investigation of the effect of rare-earth ions (Ln^{3+}) nature on the posistor properties of ($Ba_{1-X}Ln_X^{3+}$)TiO_3. Key Eng Mater 132:1313–1316

Belous AG, V'yunov OI, Kovalenko LL, Buscaglia V, Viviani M, Nanni P (2003) Effect of isovalent Ba-site substitutions on the properties of ($Ba_{1-x-y}M_yY_x$)TiO_3 (M = Ca, Sr, Pb) PTCR ceramics. Inorg Mater 39(2):133–138

Belous A, V'yunov O, Glinchuk M, Laguta V, Makovez D (2008) Redox processes at grain boundaries in barium titanate-based polycrystalline ferroelectrics semiconductors. J Mater Sci 43(9):3320–3326

Buscaglia V et al (2006) Grain size and grain boundary-related effects on the properties of nanocrystalline barium titanate ceramics. J Eur Ceram Soc 26(14):2889–2898

Dawber M, Scott JF, Hartmann AJ (2001) Effect of donor and acceptor dopants on Schottky barrier heights and vacancy concentrations in barium strontium titanate. J Eur Ceram Soc 21(10):1633–1636

Drofenik M (1993) Origin of the grain growth anomaly in donor-doped barium titanate. J Am Ceram Soc 76(1):123–128

Drofenik M, Makovec D, Zajc I, Langhammer HT (2002) Anomalous grain growth in donor-doped barium titanate with excess barium oxide. J Am Ceram Soc 85(3):653–660

Dumas J, Schlenker C, Marcus J, Buder R (1983) Nonlinear conductivity and noise in the quasi one-dimensional blue bronze $K_{0.30}MoO_3$. Phys Rev Lett 50(10):757–760

Fricbergs VY (1971) Phase transitions in ferroelectrics. Zinatne, Riga

Glinchuk MD, Bykov IP, Kornienko SM, Laguta VV, Slipenyuk AM, Bilous AG et al (2000) Influence of impurities on the properties of rare-earth-doped barium-titanate ceramics. J Mater Chem 10(4):941–947

Guillemet-Fritsch S, Valdez-Nava Z, Tenailleau C, Lebey T, Durand B, Chane-Ching JY (2008) Colossal permittivity in ultrafine grain size $BaTiO_{3-x}$ and $Ba_{0.95}La_{0.05}TiO_{3-x}$ materials. Adv Mater 20(3):551–555

Hess HF, DeConde K, Rosenbaum T, Thomas G (1982) Giant dielectric constants at the approach to the insulator-metal transition. Phys Rev B 25(8):5578–5580

Hirose Naohiro, West Anthony R (1996) Impedance spectroscopy of undoped $BaTiO_3$ ceramics. J Am Ceram Soc 79(6):1633–1641

Hou Y, Yang L, Qian X, Zhang T, Zhang Q (2016) Electrocaloric response near room temperature in Zr- and Sn-doped $BaTiO_3$ systems. Phil Trans R Soc A 374(2074):20160055

Krohns S, Lunkenheimer P, Kant C, Pronin A, Brom H, Nugroho A et al (2009) Colossal dielectric constant up to gigahertz at room temperature. Appl Phys Lett 94(12):122903–122934

Littlewood PB (1987) Screened dielectric response of sliding charge-density waves. Phys Rev B 36(6):3108–3116

Lunkenheimer P, Bobnar V, Pronin A, Ritus A, Volkov A, Loidl A (2002) Origin of apparent colossal dielectric constants. Phys Rev B 66(5):052105-1–052105-4

Lunkenheimer P, Krohns S, Riegg S, Ebbinghaus S, Reller A, Loidl A (2009) Colossal dielectric constants in transition-metal oxides. Eur Phys J Spec Top 180(1):61–89

Marikutsa A, Rumyantseva M, Baranchikov A, Gaskov A (2015) Nanocrystalline $BaSnO_3$ as an alternative gas sensor material: surface reactivity and high sensitivity to SO_2. Materials 8(9):6437–6454

Nikolsky BP (1982) Handbook of chemist. T. 1: General information, structure of substance, properties of the most important substances, laboratory equipment. Chemistry, Moscow-Leningrad, p 333

Okadzaki K (1976) Ceramic dielectric technologies [Russian translation]. Energy, Moscow, p 130

Sluyters-Rehbach M (1994) Impedances of electrochemical systems: terminology, nomenclature and representation-part I: cells with metal electrodes and liquid solutions (IUPAC Recommendations 1994). Pure Appl Chem 66(9):1831–1891

Tilley RJD (2006) Crystals and crystal structures. Wiley, Chichester, p 219

Toropov NA (1969) Diagrams of the state of silicate systems. A handbook. Issue 1. Nauka, Leningrad, p 385

V'yunov OI, Kovalenko LL, Belous AG, Belyakov VN (2003a) Effect of the distribution of manganese ions on the properties of Mn-doped (Ba,Y)TiO_3 PTCR ceramics. Inorg Mater 39(2):190–197

V'yunov OI, Kovalenko LL, Belous AG (2003b) The effect of isovalent substitutions and dopants of 3d-metals on the properties of ferroelectrics-semiconductors. Condens Matter Phys 6(2):213–220

V'yunov OI, Kovalenko LL, Belous AG (2006) Electrical properties of $BaTi_{1-x}M_xO_3$ (M = Nb, Ta, Mo, W) ceramics. Inorg Mater 42(12):1363–1368

V'yunov OI, Reshytko BA, Belous AG (2017) Synthesis and properties of semiconducting $BaTiO_3$ with colossal permittivity. Ukr Khim Zh 83(7):42–50

Von Hippel A, Breckenridge R, Chesley F, Tisza L (1946) High dielectric constant ceramics. Ind Eng Chem 38(11):1097–1109

Vul B, Guro G, Ivanchik I (1973) Encountering domains in ferroelectrics. Ferroelectrics 6(1):29–31

Wang DY (1994) Electric and dielectric properties of barium titanate Schottky barrier diodes. J Am Ceram Soc 77(4):897–910

Wu Y, Miao J, Liu Z, Li Y (2015) Colossal permittivity and dielectric relaxations in $BaTi_{0.99}(Nb_{0.5}Ga_{0.5})_{0.02}O_3$ ceramics. Ceram Int 41:S846–S850

Wu M, Yu S, He L, Yang L, Zhang W (2017) High quality transparent conductive Ag-based barium stannate multilayer flexible thin films. Sci Rep 7(1):103

Xiaoyong W, Yujun F, Xi Y (2003) Dielectric relaxation behavior in barium stannate titanate ferroelectric ceramics with diffused phase transition. Appl Phys Lett 83(10):2031–2033

Xue LA, Chen Y, Brook RJ (1988) The influence of ionic radii on the incorporation of trivalent dopants into $BaTiO_3$. Mater Sci Eng B 1(2):193–201

Yang X, Li D, Ren Z, Zeng R, Gong S, Zhou D et al (2016) Colossal dielectric performance of pure barium titanate ceramics consolidated by spark plasma sintering. RSC Adv 6(79):75422–75429

Yasuda N, Ohwa H, Asano S (1996) Dielectric properties and phase transitions of $Ba(Ti_{1-x}Sn_x)O_3$ solid solution. Jpn J Appl Phys 35(9S):5099

Zheng H, Weng W, Han G, Du P (2013) Colossal permittivity and variable-range-hopping conduction of polarons in $Ni_{0.5}Zn_{0.5}Fe_2O_4$ ceramic. J Phys Chem C 117(25):12966–12972